Supplementary Information (SI)

Sub-zero self-healable and fatigue resistant conductive ionoelastomers for sensorized soft pneumatic robots

Yang Wang*, Zhanwei Wang, Fatma Demir, Yinxin Cai, Zijin Liu, Jing Ren, Guy Van Assche, Shengjie Ling*, Bram Vanderborght*, Seppe Terryn

Supplementary Note 1. The derivation of SPA content within PSSFIE.

According to the Scheme 1 in the main text, the reaction can be simplified into $RCOO^- + H^+ \rightleftharpoons RCOOH$. And because the pKa of PAA is 4.2, acid dissociation constant of PAA can be derived:

$$Ka\ (RCOOH) = \frac{[RCOO^-][H^+]}{[RCOOH]} = 10^{-pKa} \quad (1)$$

$$-pKa = lg^{[H^+]} + lg\frac{[RCOO^-]}{[RCOOH]} \quad (2)$$

$$lg\frac{[RCOO^-]}{[RCOOH]} = pH - pKa \quad (3)$$

$$\frac{n(SPA)}{n(PAA)} = 10^{pH-pKa} \quad (4)$$

Owing to the pH result of PSSFIE which was close to 7, so $\frac{n(SPA)}{n(PAA)}$ was greater than 100, showcasing that SPA mainly exists in PSSFIE.

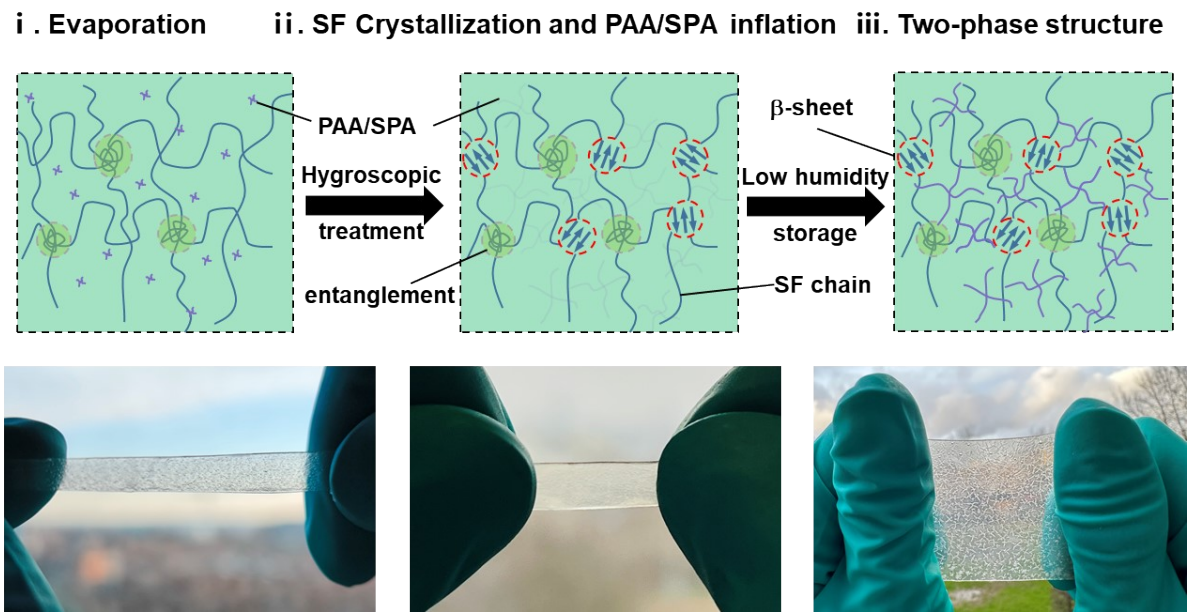

Fig. S1 Schematic illustration of preparation process of PSSFIE and corresponding photographs showing each stage of the process.

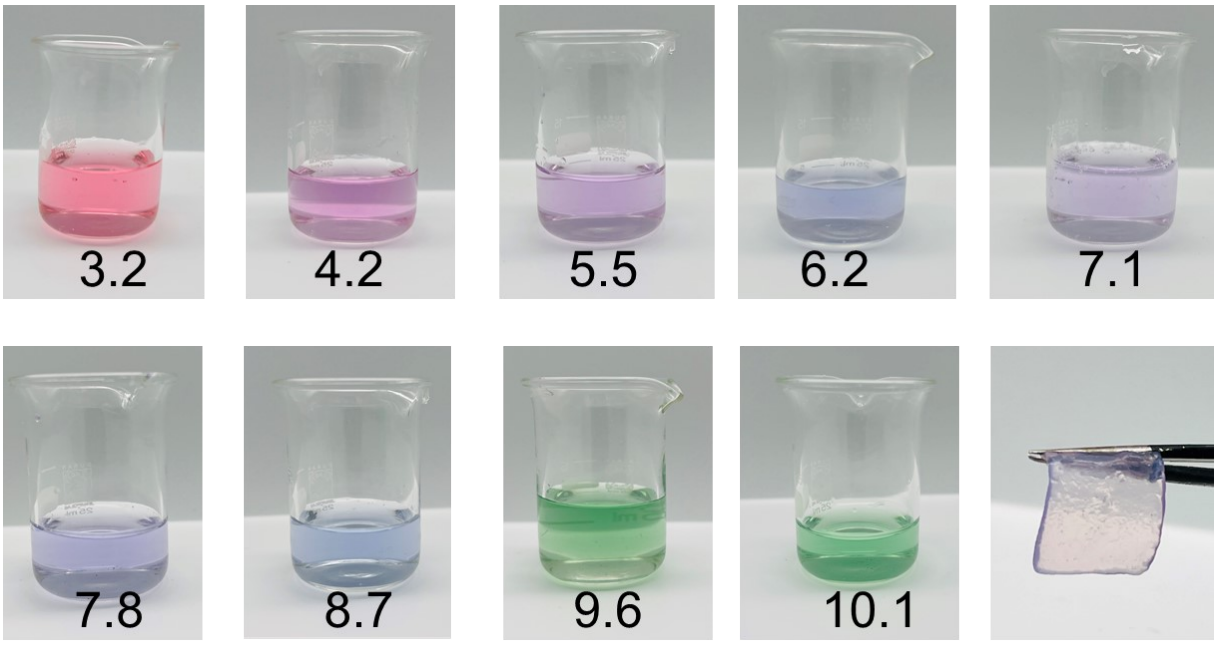

Fig. S2 The photographs of varied colored solutions across a range of pH conditions using a boiled red cabbage aqueous solution as a pH indicator and photograph of PSSFIE after immersed in the boiled red cabbage aqueous solution.

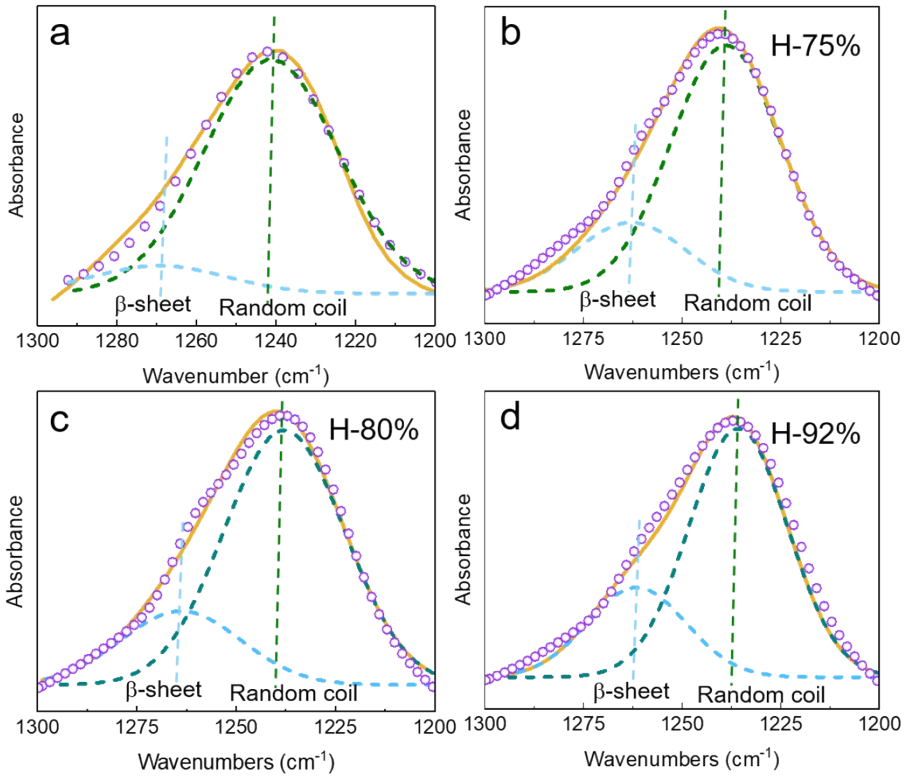

Fig. S3 Deconvolution results of the amide III band of the PSSFIE before (a) and with various hygroscopic treatments (b-d).

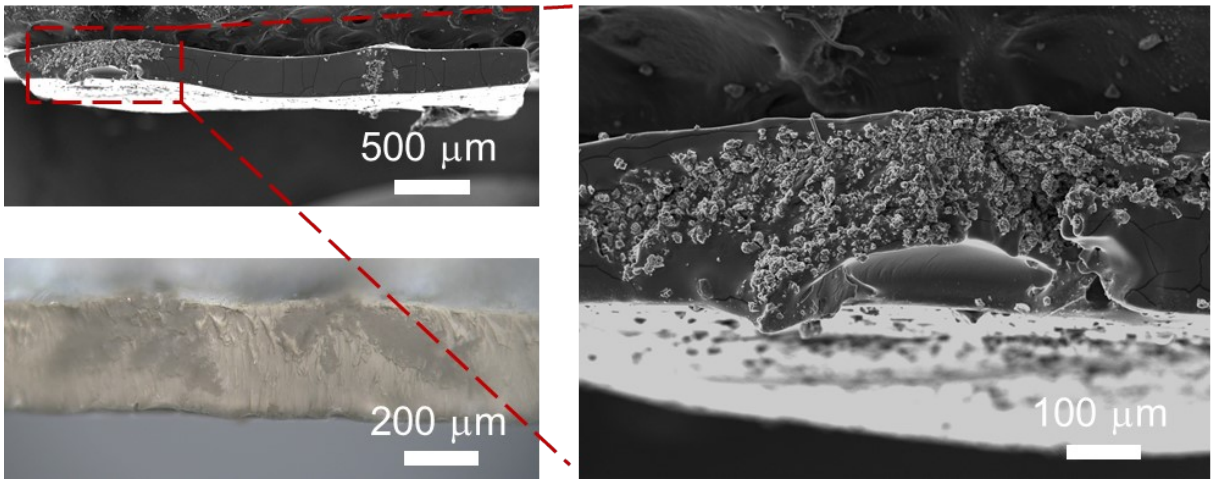

Fig. S4 Cross-sectional SEM and microscopic images of PSSFIE.

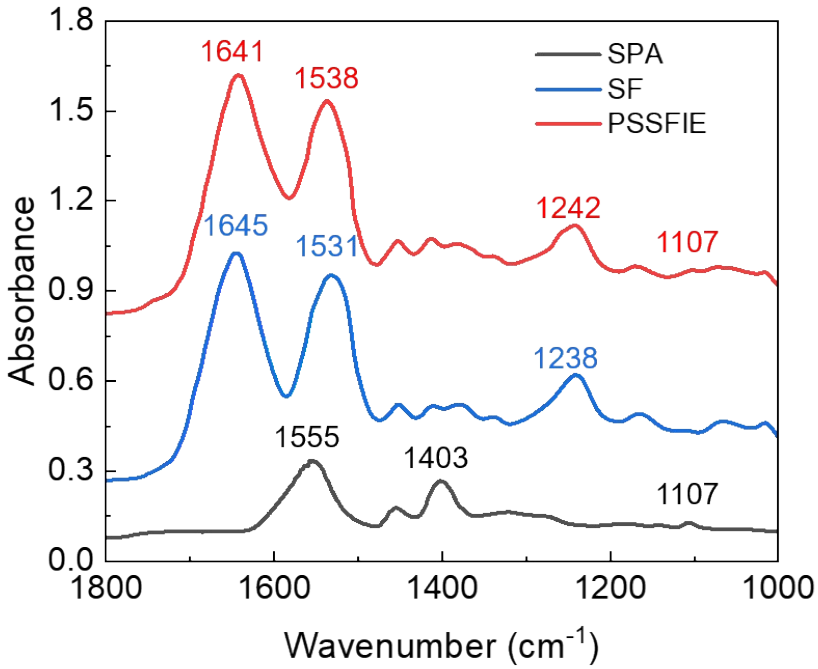

Fig. S5 ATR-FTIR spectra of sodium polyacrylate (SPA), pure silk fibroin (SF) film and PSSFIE.

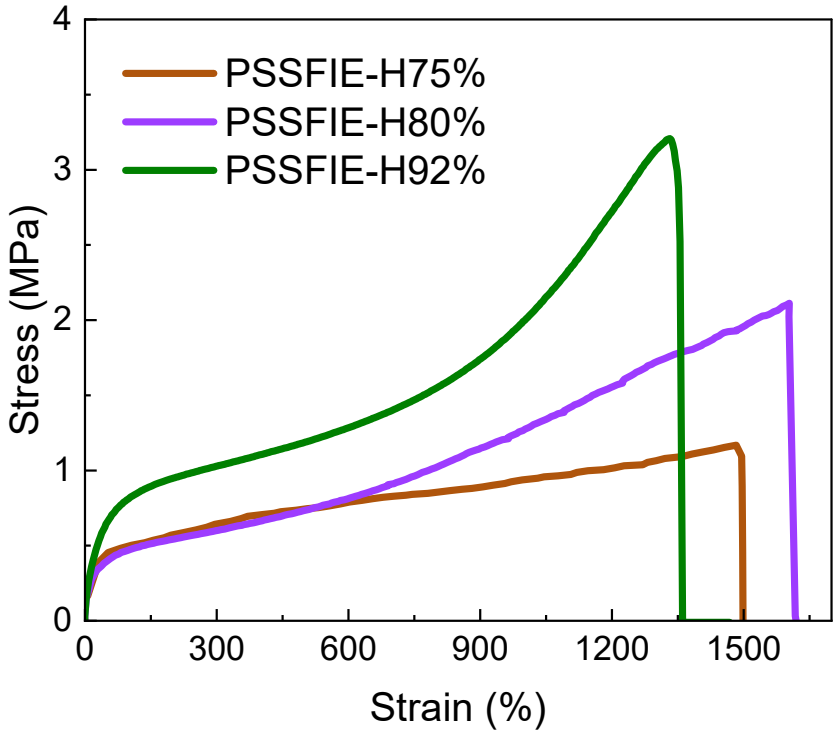

Fig. S6 Stress-strain curves of PSSFIE under various hygroscopic treatments.

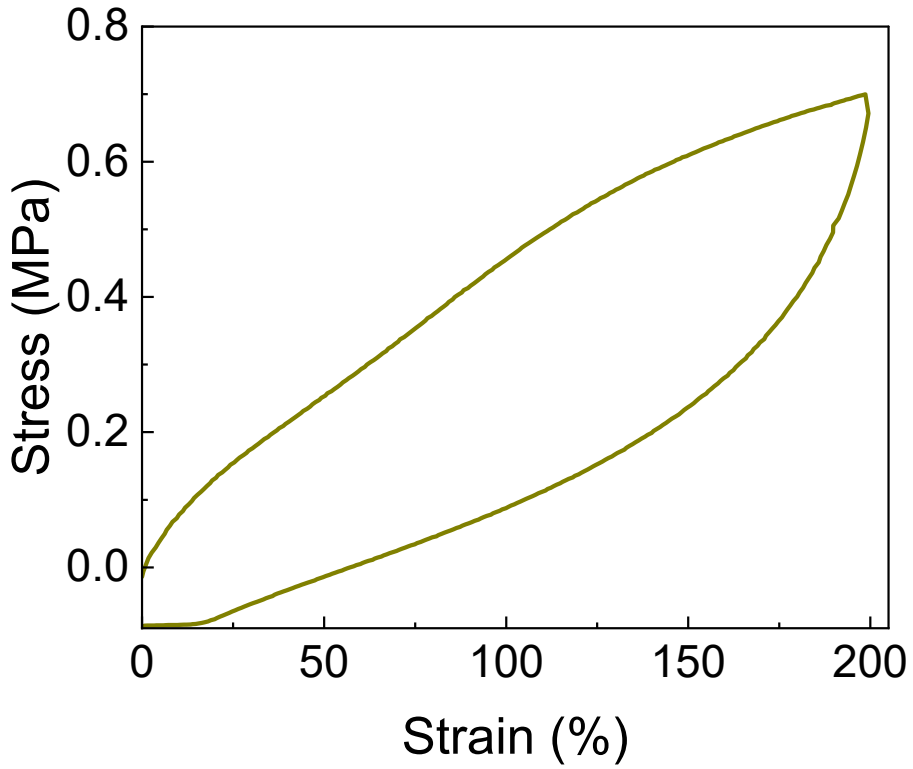

Fig. S7 The first cyclic stress–strain curve of the PSSFIE with a stretch amplitude of 200%.

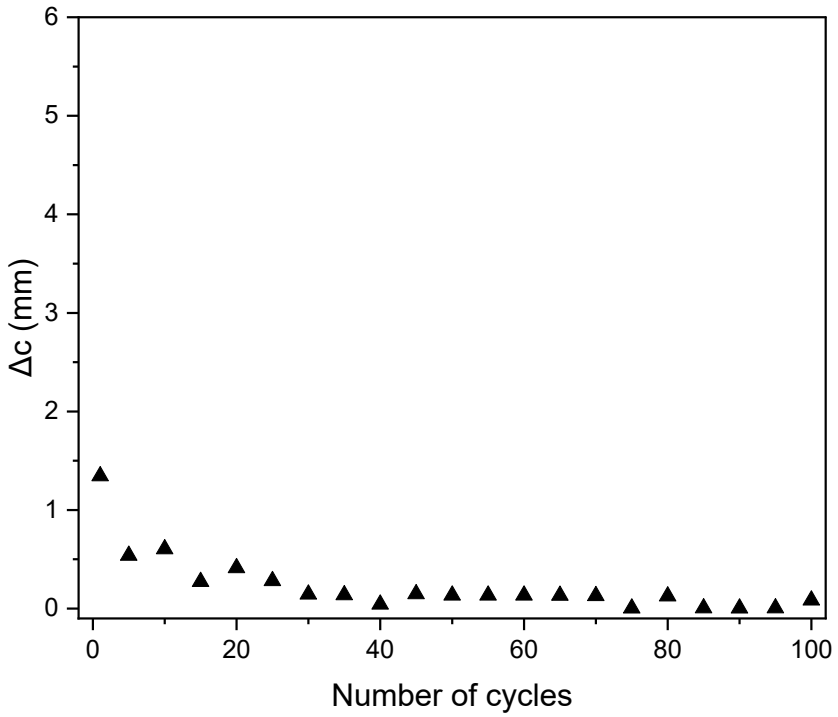

Fig. S8 The extension of the crack (Δc) of PSSFIE within 100 cycles.

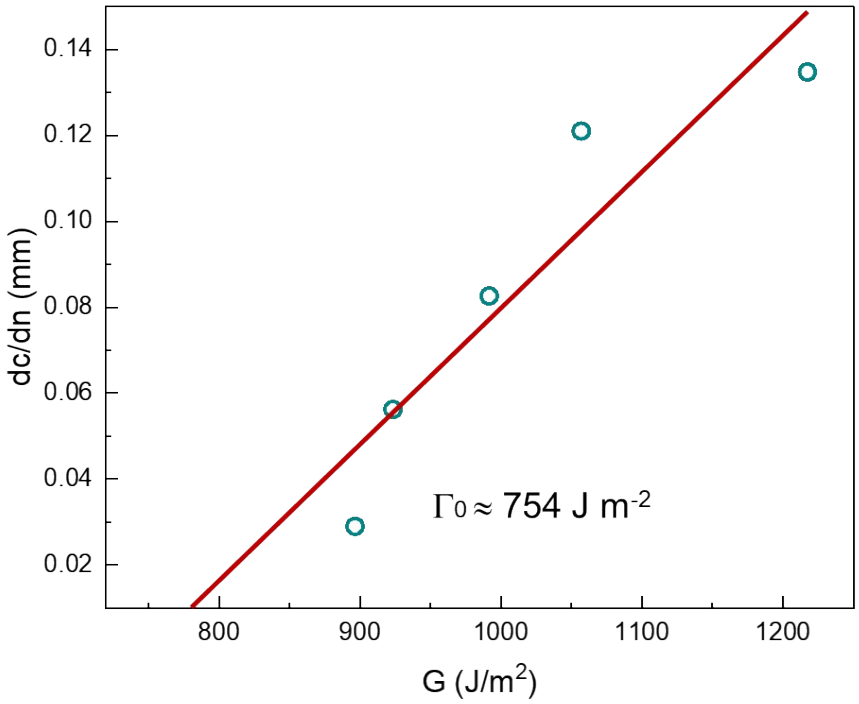

Fig. S9 Fatigue threshold Γ_0 of PSSFIE.

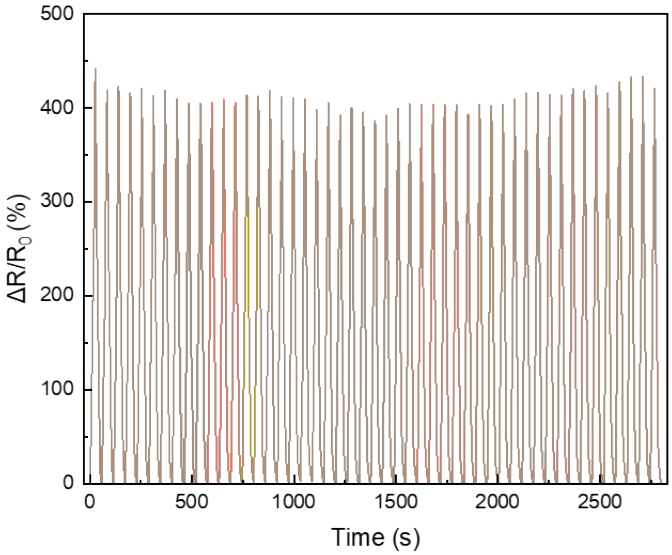

Fig. S10 The relative change in resistance curve of PSSFIE with a stretch amplitude of 200% over 50 cycles.

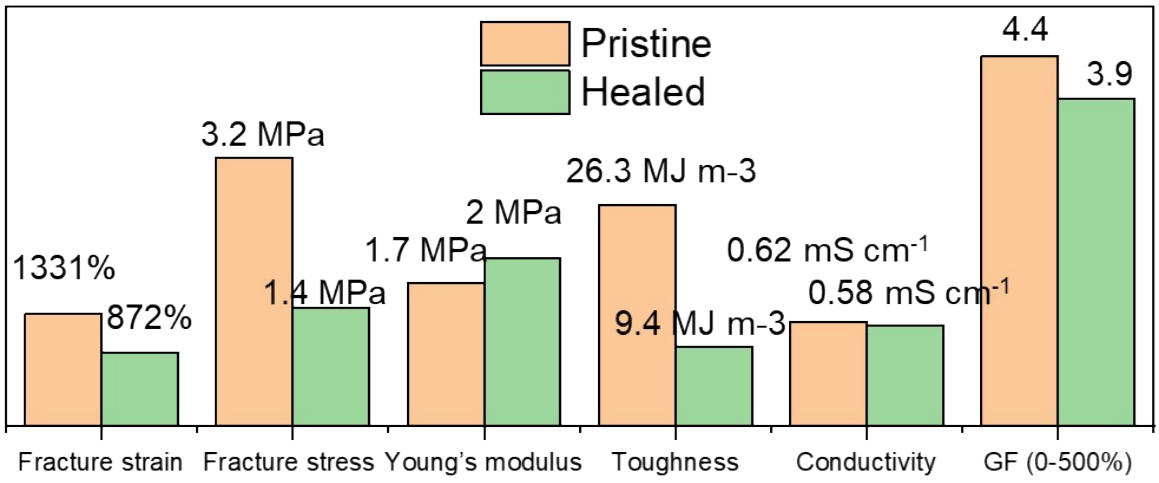

Fig. S11 Block chart showing healing efficiencies of PSSFIE based onfracture strain, fracture stress, Young's modulus, toughness, Conductivity, and GF.

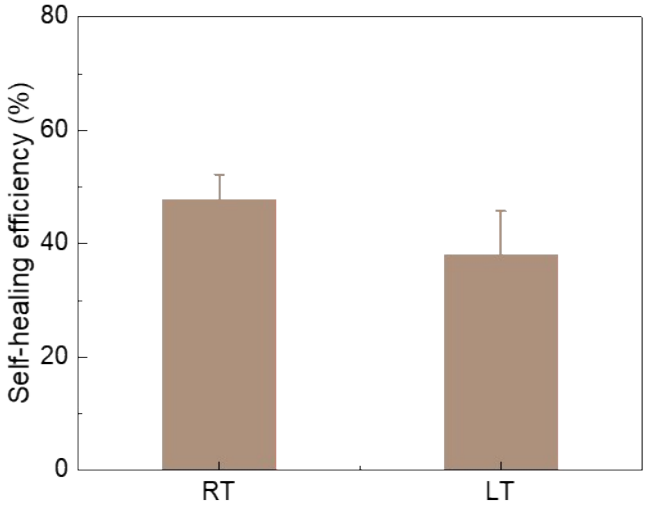

Fig. S12 The self-healing efficiency of PSSFIE self-healed at room temperature (RT) and low temperature (LT, -20°C).

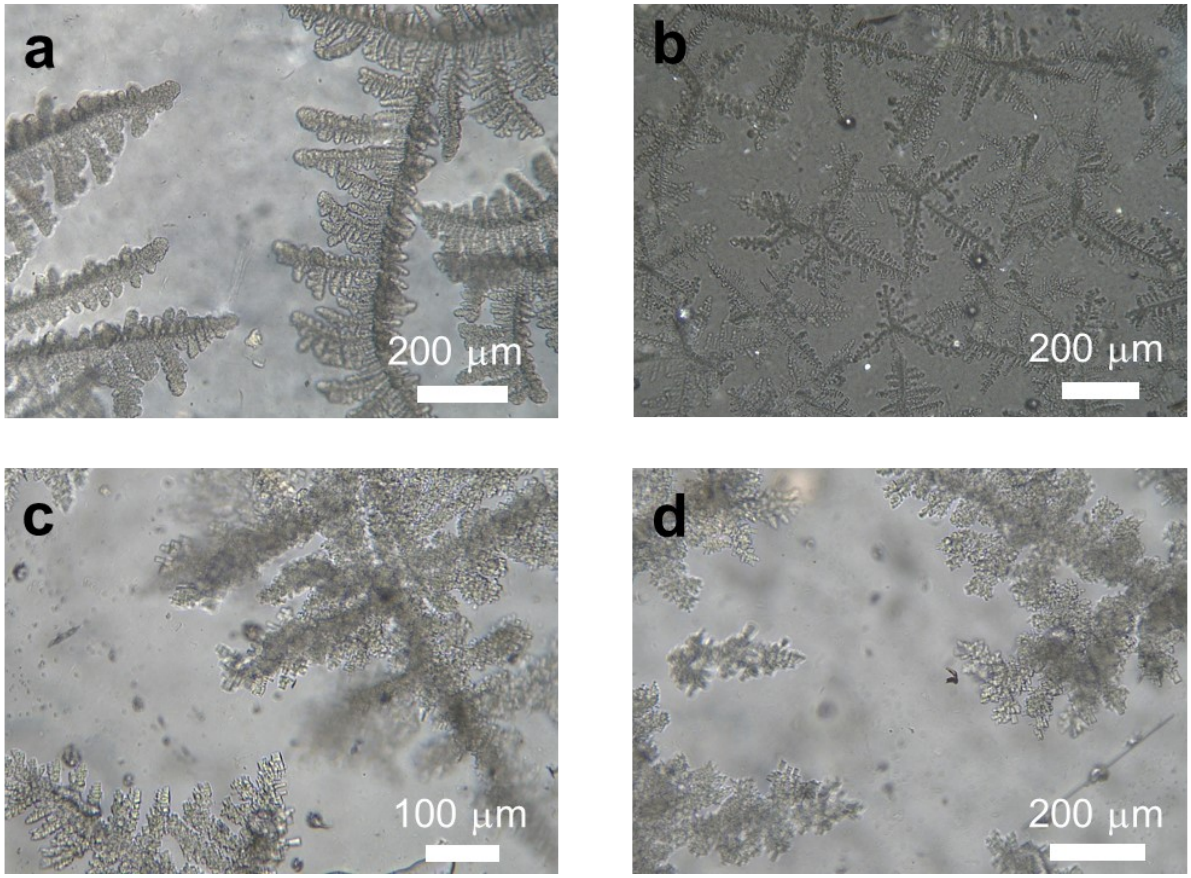

Fig. S13 The microscopic images of exposed (a, b) and sealed (c, d) PSSFIE specimens showing morphology changes before and after staying at the environment of -20 °C for 3 days.

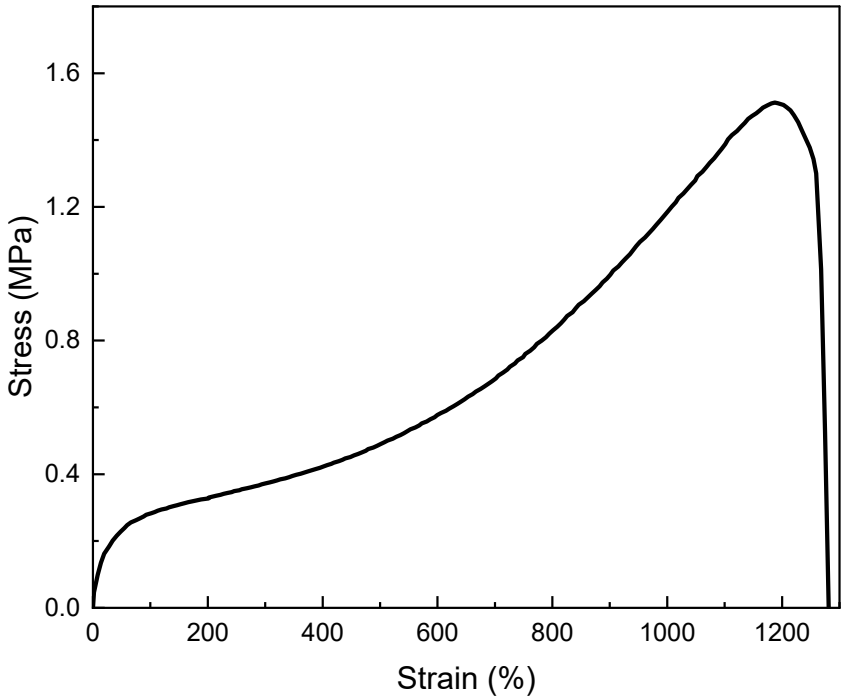

Fig. S14 The stress-strain curve of PSSFIE after self-healing in -20°C for 3 days.

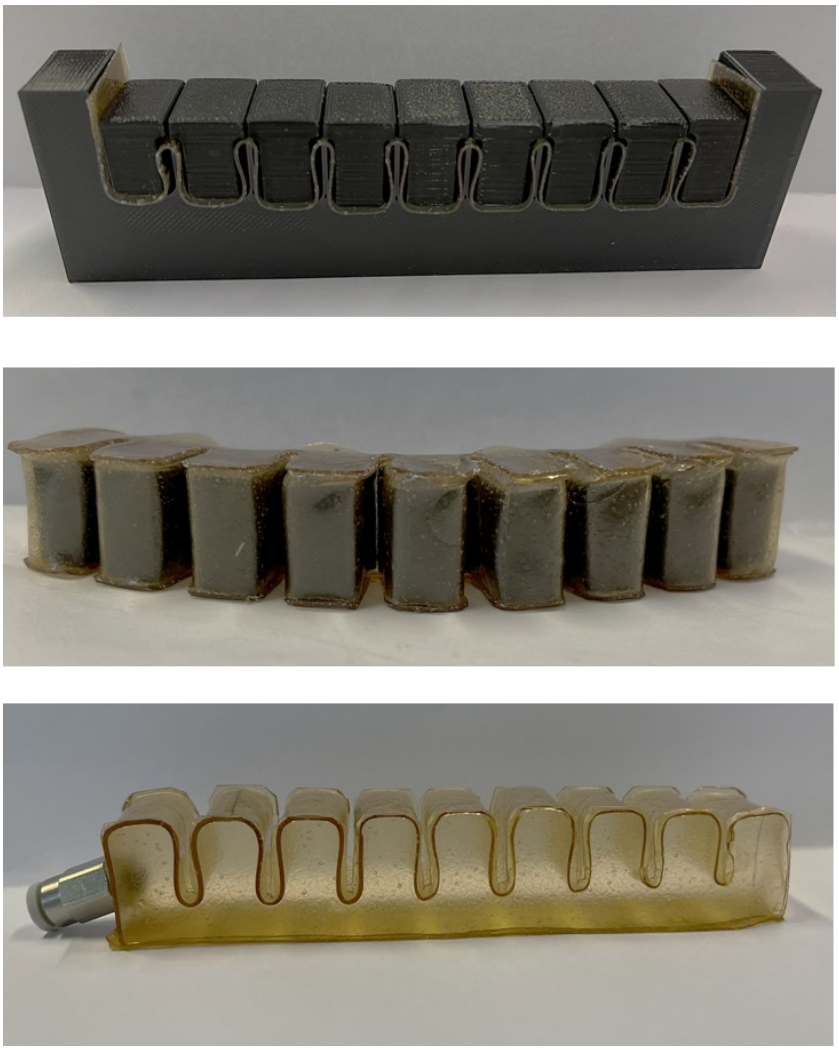

Fig. S15 The manufacturing of the PSSFIE-based soft fingers.

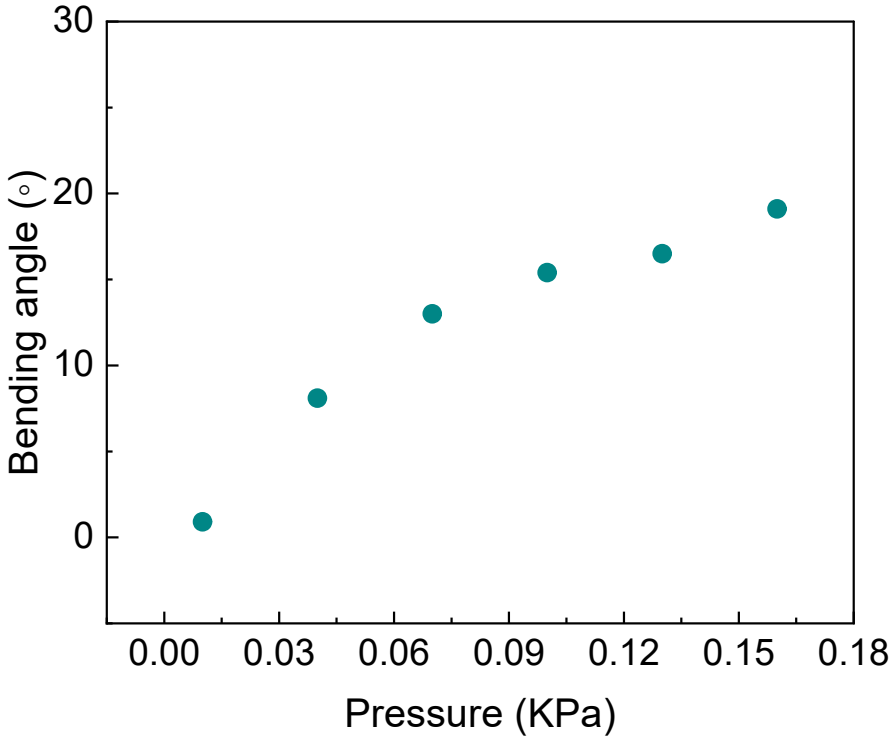

Fig. S16 The bending angle of damaged-healed PSSFIE-base soft fingers with the change of pressure at freezing temperature (0°C).